Unsymmetrical Per-Phase Control for Reactive Power-Sharing Enhancement in Unbalanced Islanded Microgrids

Dalia Yousri ⓘ, Hany E. Z. Farag ⓘ, *Senior Member, IEEE*, Hatem H. Zeineldin ⓘ, *Senior Member, IEEE*, Ahmed Al-Durra ⓘ, *Senior Member, IEEE*, and Ehab F. El-Saadany ⓘ, *Fellow, IEEE*

Abstract—Ensuring the cost-effective operation of an unbalanced islanded microgrid (UBIMG) hinges on achieving a proportional power sharing relative to the capacity of the connected distributed energy resource units (DERs). However, inherent characteristics of UBIMG, such as heterogeneous line impedance and unbalanced loads, inevitably result in mismatching the reactive power-sharing (RPS) among the droop-controlled DERs. As a solution, this article introduces an advanced control scheme that combines unsymmetrical per-phase droop control with unsymmetrical per-phase virtual impedance, referred to as unsymmetrical per-phase droop-virtual impedance control (USPDVIC), to enhance the RPS among DERs within the UBIMG. To determine the settings of the proposed control scheme, this study formulates a multiobjective optimization approach to minimize the average generation costs and mismatching in the per-phase RPS within the UBIMG across a set of operating states simultaneously. The performance of the proposed USPDVIC is comprehensively evaluated within a parallel architecture UBIMG and a radial UBIMG-based IEEE 13-bus, IEEE 34-bus, and IEEE 123-bus benchmark systems under various states of operation. These states include changes in loading conditions, plug-and-play of DERs, and system reconfiguration and partitioning. The results, along with comparisons to existing literature, provide solid evidence for the effectiveness of the proposed control scheme in improving the per-phase RPS among the parallel-connected and dispersed DERs within UBIMGs.

Index Terms—Decentralized approach, reactive power-sharing (RPS), unbalanced microgrids, unsymmetrical per-phase droop control, unsymmetrical per-phase virtual impedance.

I. INTRODUCTION

RECENTLY, there has been a notable surge in the deployment and utilization of distributed energy resource units (DERs), which could be strategically assembled to form microgrids. One key attribute of microgrids is their capability to operate in grid-connected and islanding modes. In the islanded microgrids, the connected inverters-based DERs play a crucial role in sustaining appropriate frequency and voltage levels while ensuring accurate power sharing of the load demand in proportion to their capacities and power factor limits. The precision in power sharing is paramount to the reliable and efficient functioning of the islanded microgrids. Consequently, implementing power-sharing controllers is essential in ensuring that each DER contributes an amount of power that directly aligns with its designated power rating, all while maintaining power delivery within its nominal capacity during steady-state operation [1].

The widely adopted method for autonomously managing power-sharing among DERs in islanded microgrids is traditional frequency and voltage droop control (TDC) that mimics synchronous generators. Although the traditional power-frequency $(P - f)$ droop control achieves proper active power-sharing, it has been observed that the traditional reactive power-voltage magnitude $(Q - V)$ droop has severe restraints associated with reactive power-sharing (RPS) [2]. When the distribution system at which an unbalanced islanded microgrid (UBIMG) is formed has heterogeneous line impedances coupling with a substantial presence of unbalanced three-phase and single-phase loads, the implementation of the TDC leads to a notable reduction in the accuracy of RPS. The primary issue stemming from the mismatch in the RPS is the emergence of operation issues, primarily caused by circulating currents within the inverters of the UBIMG. As a result, the system's reliability is compromised, and specific inverters may be exposed to overload conditions.

This article has been accepted for inclusion in a future issue of this journal. Content is final as presented, with the exception of pagination.

2   IEEE TRANSACTIONS ON INDUSTRIAL INFORMATICS

This exposure to overload conditions can activate protective mechanisms that can lead to unintended disturbance that impact the overall performance and reliability of the UBIMG [3].

Addressing the operation issues stemming from the mismatching in RPS has garnered substantial attention within the existing literature. To this end, various methodologies have been introduced, which can be clustered into two main groups: communication-based and communicationless procedures. Within the realm of communication-based approaches, numerous schemes were proposed, including injecting an extra small ac signal (SACS) in the output voltage of each DER [4], implementing distributed secondary control to determine virtual output impedance [5], and event-trigger secondary control schemes as in [6] and [7]. Nonetheless, communication-based procedures possess several limitations, including i) their sensitivity to the communication delay that impacts the quality of power-sharing and ii) their infrastructure complexity. Furthermore, the reliability of communication-based approaches is compromised when communication links are interrupted [8]. Recently, the work in [9] introduced a predictive voltage hierarchical controller as an alternative solution to address the limitations associated with communication delay and data loss to enhance voltage and power sharing among distributed generations.

Communicationless approaches have been identified as a more intriguing alternative solution, yet they are more challenging as they only use local measurements. The first adopted communicationless approaches for RPS were based on an extension application for the TDC [10]. For example, the works in [11] improved the voltage restoration approach for the $(Q - \dot{V})$ droop control to minimize the deviation in the RPS. Yet, the approach did not control the steady-state voltage deviation that may cause voltage issues in the islanded microgrid. An advanced TDC approach was proposed in [3] to address the drawbacks of the $(Q - \dot{V})$ droop control. However, the advanced TDC approach assumed knowledge of all cables' impedance; moreover, it was evaluated on a basic fixed parallel architecture islanded microgrid with only common balanced loads without being examined under disturbances, e.g., sudden outage of DERs or loads.

Coupling the virtual impedance with the droop control (VIC) to improve the RPS is the other widely implemented communicationless approach. For example, the works in [12] proposed an adaptive VIC (AVIC) that is proportional to the generated reactive power through an adaptive coefficient; as a result, an improved reactive power virtual impedance (Q-vi) droop was adopted. However, it was observed that the unsuitable adjustment for this proportional adaptive coefficient led to some instability phenomena [13]. The authors in [14] used the DER's reactive power output and the terminal voltage to estimate the VIC for improving the RPS accuracy. This scheme used local measurements without requiring the line impedance value. Yet, it was examined on a basic parallel architecture islanded microgrid with only balanced loads. In [15], the authors inserted a virtual capacitor (VCC) parallel to the inverter terminals to enhance RPS. The improper adjusting of the virtual capacitor coefficient

can cause a system stability issue [13]. The works in [16] used a linear function of the DER's current output to provide an AVIC to achieve better RPS with a balanced load. Although the performance of the previous schemes is considered promising for a balanced islanded microgrid, it cannot remove the RPS error with connecting unbalanced loads, as they may cause negative and zero-sequence currents to flow, which leads to oscillatory components in the power profiles [17].

To tackle the challenge of circulating power within the UBIMG, various control strategies have been explored using the sequence component separation approach. For instance, using virtual conductance against negative sequence power, based on the TDC, was adopted in [18]. A linearly varying AVIC correlated with the negative sequence output currents of DERs was designed in [19]. In addition, a negative-sequence VIC was introduced in [20] to mitigate the negative-sequence circulating current. Nevertheless, certain limitations need to be acknowledged: i) the neglect of the zero-sequence component of current in the VIC and AVIC implementation; and ii) the disregard of the fact that the heterogeneous line impedance in UBIMG impacts both positive and negative-sequence RPS [21]. As a result, the recent exploration of a per-phase-based control scheme is notable for its simplicity and reliability. The symmetric per-phase-based inverse droop control scheme (SPDC) complemented by secondary control was devised in [22]. This scheme aimed to regulate frequency and provide balanced voltage to the load terminals of the low-voltage (LV) UBIMG. However, it is important to note that this approach relies on communication. In similar research, the works in [23] applied an SPDC to the droop control scheme to enhance active power-sharing among parallel-connected DERs for resistive unbalanced loads. Nevertheless, certain assumptions made in this work warrant consideration as they impact the system's response accuracy. Specifically, these assumptions involve 1) employing symmetrical per-phase droop gains, which can lead to voltage deviations among phases due to unequal (imbalance) power flow within the phases of the UBIMG, and 2) the assumption of homogeneous line impedance, neglecting the study of mismatched impacts stemming from heterogeneous line impedance.

In light of the previously discussed literature, while valuable insights have been gleaned from these studies, they may not adequately capture the multifaceted reality of actual microgrids, which often involve diverse load types and configurations. Several notable gaps warrant careful consideration and further investigation.

1) Most control schemes have been evaluated within the confines of a simplified fixed parallel architecture for islanded microgrids with balanced loads. However, the islanded microgrid is expected to extend to large distribution feeders with dispersed sources and unbalanced single and three-phase loads.

2) Many studies have neglected the impact of heterogeneity on the line impedance of UBIMG, yet it is a factor that can substantially influence the microgrid operation.

3) Existing evaluations have adhered to rather simplistic scenarios, often devoid of the dynamic effects stemming

from DERs being added or removed from the microgrid and changes in the overall system configuration.

4) Previous studies have used solo symmetric control parameters; however, they do not fully address the issues caused by the heterogeneity in line impedance and the imbalance of per-phase power flow in the UBIMG.

It is imperative to bridge these gaps to advance an understanding of UBIMG control and its suitability for diverse and real-world applications. Accordingly, developing a control scheme that exhibits adaptability and effectiveness in navigating the inherent features of UBIMG is required.

To address these identified research gaps, this study proposes an advanced control scheme designed to enhance the RPS in UBIMG. Taking into account the inherent features of UBIMG, such as heterogeneous line impedance and the presence of single- and unbalanced three-phase loads, the proposed control scheme integrates unsymmetrical per-phase droop control (USPDC) with unsymmetrical per-phase virtual impedance (USPVIC), collectively referred to as unsymmetrical per-phase droop-virtual impedance control (USPDVIC). The introduction of this unsymmetrical controller framework aims to effectively manage variations in power flow across phases and account for heterogeneity in line impedance within the UBIMG. In alignment with the principles of a communicationless approach, the study formulates a multiobjective optimization problem to determine a unique set of appropriate settings for the USPDVIC. Such settings, including per-phase droop gains and per-phase virtual impedance, simultaneously accommodate a range of operating states. It is worth mentioning that this approach minimizes the need for frequent updates to the controller settings, as the identified unique settings are designed to fit a set of operating conditions simultaneously. The formulated multiobjective optimization problem aims to achieve two key objectives: 1) minimize average generation costs for economic dispatch and 2) minimize average mismatches in RPS for enhanced system reliability. The efficiency of the proposed USPDVIC is comprehensively evaluated within a parallel architecture UBIMG and a radial UBIMG-based IEEE 13-bus, IEEE 34-bus, and IEEE 123-bus benchmark systems under various states of operation. The main contributions and advantages of this work are summarized as follows.

1) Developing a novel USPDVIC to minimize mismatching in RPS within the UBIMG. Proposing an unsymmetrical per-phased-based controller in this work establishes a framework for managing variations in power flow across phases and heterogeneity in line impedance within the UBIMG, which is not considered in [4–23].

2) Formulating a multiobjective optimization problem to identify a distinct set of USPDVIC settings suitable for various operational states simultaneously. This approach offers an alternative solution to mitigate the need for frequent updates in controller settings, addressing the limitations of communication-based approaches as outlined in existing literature [4–7].
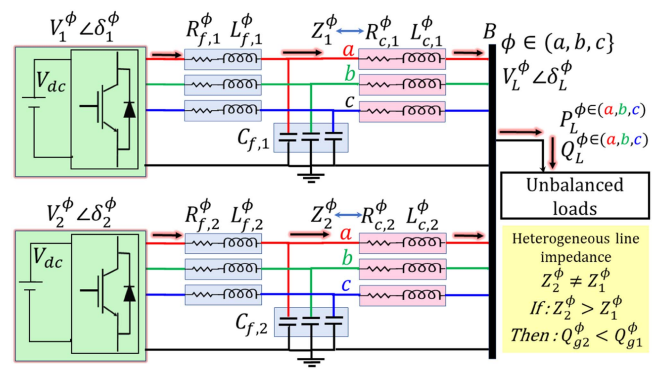
Fig. 1. UBIMG-based two-parallel-connected-dispatchable DERs architecture with heterogeneous line impedance $Z_2^\phi \neq Z_1^\phi$ (assuming $Z_2^\phi > Z_1^\phi$).

II. INVESTIGATE SYMMETRIC VERSUS UNSYMMETRICAL-BASED CONTROL SCHEMES IN RPS WITHIN UBIMG

To investigate the basic principles of implementing the symmetrical and unsymmetrical-based control schemes on RPS within UBIMG, two inverter-based UBIMG with heterogeneous line impedance where $(Z_2^\phi \neq Z_1^\phi)$, as illustrated in Fig. 1, is considered in this section. Referring to the structure shown in Fig. 1. In case X/R is high, the output reactive powers of DER_i $(i = 1, 2)$ can be derived as

$$Q_{gi}^\phi = \frac{V_i^\phi \left(V_i^\phi - V_L^\phi \cos(\triangle \delta_i^\phi)\right)}{Z_i^\phi} \quad (1)$$

where Q_{gi}^ϕ is the per-phase generated reactive power by the ith DER, $\triangle \delta_i^\phi$ is the per-phase phase difference between the terminal voltage (V_i^ϕ), and a voltage at a point of common coupling (V_L^ϕ). Usually, $\triangle \delta_i^\phi$ is assumed to be very small; accordingly, the reactive power can be rewritten as follows:

$$Q_{gi}^\phi = \frac{V_i^\phi \left(V_i^\phi - V_L^\phi\right)}{Z_i^\phi}. \quad (2)$$

The relation in (2) highlights an inverse correlation between Q_{gi}^ϕ and Z_i^ϕ. Assuming the heterogeneous lines impedance of the depicted UBIMG in Fig. 1 have values of $Z_2^\phi > Z_1^\phi$, this implies that $Q_{g2}^\phi < Q_{g1}^\phi$. Based on (2), the $(Q - V)$ droop control relation can be given as below:

$$V_i^\phi = V_o^\phi - nq_i^\phi \left(Q_{gi}^\phi - Q_o^\phi\right) \quad (3)$$

where Q_o^ϕ and V_o^ϕ represent the per-phase nominal reactive power and nominal voltage, respectively. The per-phase $(Q - V)$ droop coefficients are given by nq_i^ϕ for each phase ϕ and the ith DER.

Utilizing the relations defined in (2) and (3), Fig. 2 presents a graphical representation of the rising slopes of the reactive power-stage curves for DER_1 and DER_2 (illustrated in solid and

This article has been accepted for inclusion in a future issue of this journal. Content is final as presented, with the exception of pagination.

4   IEEE TRANSACTIONS ON INDUSTRIAL INFORMATICS

Fig. 2. RPS by two DERs of UBIMG in Fig. 1(a) without VIC, (b) with symmetrical VIC, (c) with USPVIC, and (d) RPS of phase a using USPDC+USPVIC.

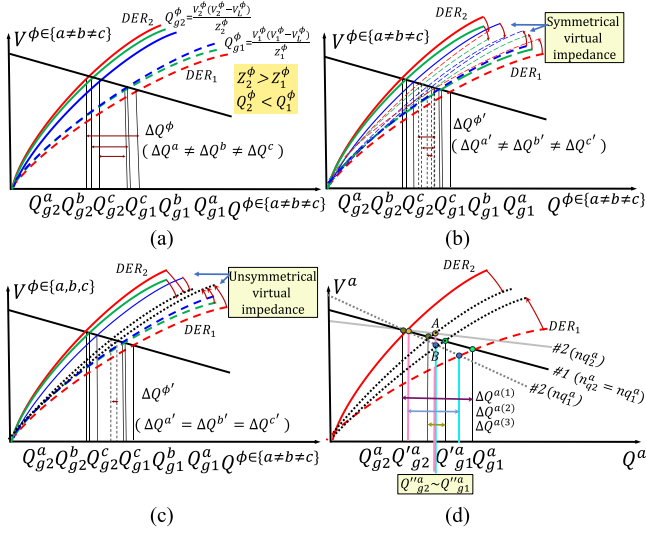dashed red, green, and black to represent "a, b, c" phases), along with the $(Q - V)$ droop control characteristic. This representation is provided within the context of the UBIMG shown in Fig. 1. To elaborate on the correlations between RPS and line impedance, the assumption is made that the impedance of the first feeder is less than that of the second feeder in the UBIMG of Fig. 1, i.e., $Z_2^\phi > Z_1^\phi$. This implies that $Q_{g2}^\phi < Q_{g1}^\phi$, as depicted in Fig. 2.

In the case where a SPDC setting (black solid line) is applied, as depicted in Fig. 2(a), the figure illustrates that the presence of heterogeneous line impedance and imbalance power distribution among the phases of the UBIMG leads to unequal mismatching in per-phase RPS, denoted as ΔQ^ϕ, where $\Delta Q^a \neq \Delta Q^b \neq \Delta Q^c$. To address this deviation, the incorporation of symmetrical per-phase VIC (SPVIC) for each phase results in updated rising slopes of the power-stage curves for DER$_1$ and DER$_2$ as visualized in Fig. 2(b). The figure demonstrates that this adjustment minimizes the deviation in per-phase RPS, now represented as $\Delta Q^{\phi'}$. However, it is important to highlight that relying solely on symmetrical settings does not completely mitigate the challenges posed by the system imbalance. Consequently, the modified $\Delta Q^{\phi'}$ values remain unequal, with $\Delta Q^{a'} \neq \Delta Q^{b'} \neq \Delta Q^{c'}$. As a result, this approach might not be the most effective means to avoid the circulating reactive power among phases and achieve precise RPS among the connected DERs within the UBIMG.

To emphasize the significance of incorporating USPVIC and USPDC within the UBIMG, consider Fig. 2(c) and (d). Fig. 2(c) illustrates the rising slopes of the per-phase power-stage curves for DER$_2$ and DER$_1$ underscore the presence of RPS mismatch among the DERs phases, denoted as $\triangle Q^{\phi \in (a,b,c)}$, where it is conceivable that $\triangle Q^a \neq \triangle Q^b \neq \triangle Q^c$. To mitigate these deviations, at this time, the USPVIC is applied to counteract the observed per-phase deviation levels to be $\triangle Q^{\phi \in (a,b,c)'}$, where it

is conceivable that $\triangle Q^a \approx \triangle Q^b \approx \triangle Q^c$ can be achieved. This corrective measure is indicated by the black dotted points in Fig. 2(c). Relying solely on USPVIC may substantially reduce the error in RPS; however, adding large values of USPVIC may distort the voltage profiles. Hence, combining USPDC with USPVIC could be a potential alternative solution to minimize the mismatch in the RPS.

For a more insightful representation, Fig. 2(d) spots the light on phase "a" of the two identical DERs and offers a visual representation of the responses obtained when solely employing USPVIC, USPDC only, and the combined utilization of both approaches (USPDVIC). The visualization presented in Fig. 2(d) helps in conveying the potential benefits of integrating these control strategies to improve the RPS. When the USPVIC is applied on phase "a" of each DER while the symmetrical droop control gains are used ($n_{qi}^a = n_{qj}^a$, depicted by #1 black solid line), the deviation in the RPS is minimized from $\triangle Q^{a(1)}$ to $\triangle Q^{a(3)}$. When the unsymmetrical droop gains ($n_{qi}^a \neq n_{qj}^a$ shown #2 gray solid and dotted lines) are applied, the deviation in the RPS is minimized from $\triangle Q^{a(1)}$ to $\triangle Q^{a(2)}$. Further, when the two approaches are combined (USPDVIC), the droop characteristic of DER$_2$ (solid gray line) interacted with the modified rising slopes of the power-stage curves for DER$_2$ (dotted black) in point A. Similarly, the droop characteristic of DER$_1$ (dotted gray line) interacted with the modified rising slopes of the power-stage curves for DER$_1$ (dotted black) in point B. The figure vividly demonstrates that the RPS achieved by the DERs at points A and B is nearly equal ($Q_{g1}^a \approx Q_{g2}^a$ as $\triangle Q^a \approx 0$). This illustration effectively underscores the potential advantages of the integrated USPDVIC in improving the accuracy of RPS.

III. STRUCTURE OF PROPOSED ADVANCED UNSYMMETRICAL PER-PHASE CONTROL SCHEME

To address the mismatch issue in RPS within the low-inertia UBIMG, the control block of the USPDVIC is presented in this section. The control block diagram is exhibited in Fig. 3, encompassing a USPDC loop, a USPVIC loop, as well as inner voltage and current control loops. The specific formulations of these loops are elucidated as follows:

In the power control loop, droop control is a widely adopted communicationless power-sharing mechanism among DER units. Various droop control formulations have been proposed in the literature, primarily differing based on the system's X/R ratio and the output impedance of the DERs. Notably, the $(d\delta_i - P_{gi}$ and $V_i - Q_{gi})$ formula has been established as suitable droop representations for medium voltage (MV) microgrids where X/R is high (highly inductive properties) [2]. The mathematical formulation of the USPDC ($d\delta_i^\phi - P_{gi}^\phi$ and $V_i^\phi - Q_{gi}^\phi$) of Fig. 3 can be expressed as follows:

$$V_i^\phi = V_o^\phi - nq_i^\phi \left(Q_{gi}^\phi - Q_0^\phi \right) \tag{4}$$

$$d\delta_i^\phi = \omega^* - mp_i^\phi \left(P_{gi}^\phi - P_0^\phi \right) \tag{5}$$

where ω^* represents the nominal angular frequency in radians per second (rad/s). The per-phase droop coefficients are given
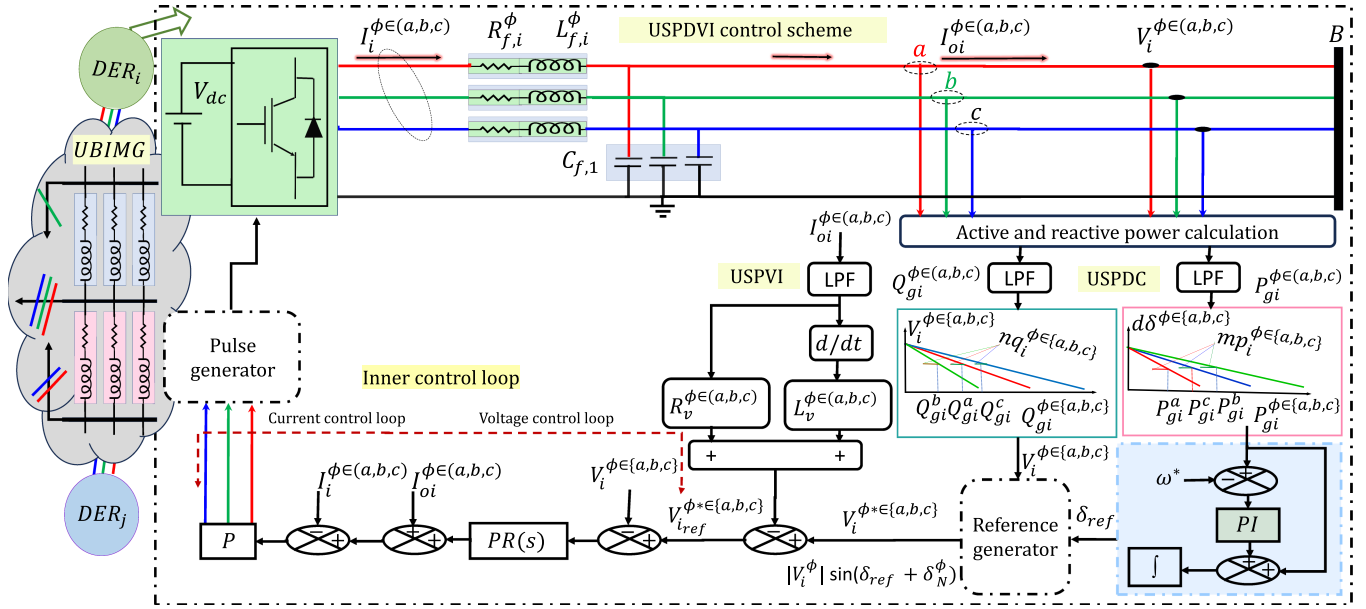
This article has been accepted for inclusion in a future issue of this journal. Content is final as presented, with the exception of pagination.

YOUSRI et al.: UNSYMMETRICAL PER-PHASE CONTROL FOR REACTIVE POWER-SHARING ENHANCEMENT   5

Fig. 3.   Control scheme of the proposed USPDVIC.

by nq_i^ϕ, mp_i^ϕ for each phase ϕ and the ith DER. To maintain the frequency within its specified boundaries of 3% from the nominal value, regarding IEEE Std 1547-2003, [24], after each load disturbance, the control scheme of Fig. 3 includes a frequency restoration block diagram. This diagram incorporates a straightforward concept that relies on the frequency deviation ($\triangle d\delta_i^\phi$), which acts upon the output of the droop controller and generates a modified frequency reference in the standard limits [25], [26]. As a result, the voltage angle reference ($\delta_{i_{ref}}$) is established by integrating the output ($d\delta_i^\phi$) from the frequency restoration block diagram, which is then used in the reference generator block [25], [26]. In the reference generator block of Fig. 3, the instantaneous reference voltage values are computed using the following formula:

$$V_i^{\phi^*} = |V_i^\phi|\sin\left(\delta_{i_{ref}} + \delta_N^\phi\right) \qquad (6)$$

where δ_N^ϕ represents the nominal phase angle that has values of $(0, -2/3\pi, 2/3\pi)$ for specific "a, b, c" phases as illustrated in Fig. 3. The proposed USPDC is enhanced with a USPVIC that is designed to regulate voltage levels. The core concept revolves around emulating a voltage drop within the controller such that the ith DER perceives the primary network [27]. This objective is achieved by multiplying the per-phase virtual resistance ($R_{v_i}^\phi$) with the output current of each respective phase ($I_{o_i}^\phi$) and also multiplying the per-phase inductive ($L_{v_i}^\phi$) with the time derivative of each phase's output current ($\frac{dI_{o_i}^\phi}{dt}$). The results of these multiplications are then subtracted from the computed reference voltage obtained from (6). To filter out oscillatory components present in the output current, a low-pass filter (LPF) is integrated into the USPVIC loop, as illustrated in Fig. 3. As a result, an updated per-phase reference voltage is generated based

on the following equation:

$$V_{i_{ref}}^{\phi^*}(t) = V_i^{\phi^*}(t) - \left(R_{v_i}^\phi I_{o_i}^\phi(t) + L_{v_i}^\phi \frac{dI_{o_i}^\phi}{dt}\right). \qquad (7)$$

The inner control loop is composed of voltage and current control loops that are structured to regulate the inverter voltage. In the block diagram of Fig. 3, the proportional-resonant controller (PR) is employed to track the sinusoidal voltage references of each phase of each DER unit. This controller is strategically positioned downstream of both the USPDC and USPVIC. The transfer function of the PR control can be mathematically represented as follows:

$$PR_i^\phi(s) = K_{pv} + \frac{K_{iv}s}{s^2 + \omega_c s + \omega_o^2} \qquad (8)$$

where K_{pv} and K_{iv} represent the proportional and integral gain factors, respectively. The parameters ω_c and ω_o correspond to the cutoff frequency and resonant frequency, respectively. The resultant output current reference, derived from the voltage control loop, is subsequently fed into the proportional controller of the current control loop with gain K_p. This action generates the references a, b, and c, which are further utilized to generate the pulse width modulation (PWM) signals required to operate the inverter. The transfer function of the proportional controller can be formulated as follows:

$$P_i^\phi = K_p. \qquad (9)$$

The proposed USPDVIC control scheme operates without communication, presenting a challenge in establishing a unique set of unsymmetrical control settings capable of adapting to multiple predefined operating states concurrently. This adaptability enhances RPS without necessitating frequent updates to the controller settings. Taking inspiration from the approach presented in [28], the strategy involves assigning a unique set

This article has been accepted for inclusion in a future issue of this journal. Content is final as presented, with the exception of pagination.

6   IEEE TRANSACTIONS ON INDUSTRIAL INFORMATICS

of control settings offline to match a predefined set of operating conditions. This approach offers a promising alternative solution to avoid the limitations of communication-based approaches. Notably, it does not necessitate frequent updates to the controller settings, which can be performed when the microgrid undergoes significant load states and/or topology changes. In these cases, it is assumed that each DER is equipped with low-bandwidth communication to facilitate the necessary updates to its control settings. Identifying such a unique set of control settings offline to align with predefined operating conditions simultaneously presents a challenge. Part of this challenge involves ensuring cost-effective operation and improved RPS without the need for frequent updates to the controller settings, which have to be addressed within the optimization process. The required settings for the proposed USPDVIC control scheme for each ith DER and the ϕth phase consist of $2 \times \phi$ plus six variables. This arises from calculating two droop parameters for each phase, denoted as nq_i^ϕ and mp_i^ϕ, and the six variables refer to the number of identified USPVI $(R_{vi}^\phi, L_{vi}^\phi)$ for each DER. Consequently, the identification process necessitates determining "12" variables for each DER in the system, which requires the formulation of an optimization problem. Therefore, the following section outlines the mathematical model of the proposed multiobjective optimization to determine a unique set of control settings that enhance the RPS in UBIMG while also achieving a cost-effective operation under a set of predefined operating states.

IV. FORMULATION OF THE IMPLEMENTED MULTIOBJECTIVE FUNCTIONS

This section outlines the mathematical formulation of two concurrent optimized objective functions to determine the unique settings of the USPDVIC $(mp_i^\phi, nq_i^\phi, R_{vi}^\phi, L_{vi}^\phi)$ that achieve cost-efficient operation while ensuring accurate RPS among the DERs within the UBIMG under a set of predefined operating states simultaneously. These functions are solved concurrently using the multiobjective optimization technique. Since the proposed control scheme is communicationless, the objective functions are optimized offline across M predefined operating states to determine a unified set of control settings that align with the set of M states simultaneously. The average generation cost and the average mismatch in per-phase RPS across the defined set of M operational states are the objective functions to be solved concurrently. This strategy enables the identification of unique control settings that align with M states without communication. The mathematical formulations of the optimized objective functions (Obj_1, Obj_2) are expressed as follows:

1) The average generation cost $(ACost)$ can be given as

$$Obj_1 \Longrightarrow ACost = \frac{1}{M} \sum_{St=1}^{M} \sum_{i=1}^{N} C_{g_{i,st}}$$

$$C_{g_{i,st}} = C_{g_i}^{FX} + \left(C_{g_i}^{O\&M} + C_{g_i}^{F} \right) P_{g_{i,st}} \qquad (10)$$

where $C_{g_i}^{FX}$, $C_{g_i}^{O\&M}$, and $C_{g_i}^{F}$ refer to the fixed cost incurred to the ith DER in \$/h, the operating/maintenance costs and the fuel cost for ith DER in \$/kWh. The $P_{g_{i,st}}$ is the total generated

power of the ith DER at the Stth state in kW. M and N are the total numbers of the considered operating states and the interconnected DER units, respectively. The fixed cost $(C_{g_i}^{FX})$ can be computed using the following expression [29]:

$$C_{g_i}^{FX} = \frac{C_{g_i}^{Cap} P_{g_i}^{C} rb_{g_i}}{T_{g_i} \times 365 \times 24 \times CF_{g_i}} \qquad (11)$$

where $C_{g_i}^{Cap}$ is the capital cost of the ith DER in \$/kW and $P_{g_i}^{C}$ is the ith DER capacity in kW. The symbols of rb_{g_i}, T_{g_i}, and CF_{g_i} denote the annual rate of benefit, the lifetime, and a capacity factor of the ith DER.

2) The average mismatch in per-phase RPS can be computed as follows:

$$Obj_2 \Longrightarrow A\triangle Q = \frac{1}{M} \sum_{St=1}^{M} \triangle Q$$

$$\triangle Q = \sum_{\phi \in a,b,c} \sum_{i=1}^{N} \sum_{j=i+1}^{N} |Q_{g_i}^\phi - Q_{g_j}^\phi| \qquad (12)$$

where $|Q_{g_i}^\phi - Q_{g_j}^\phi|$ is the absolute difference in the per-phase RPS among the ith and the jth DERs.

The optimization problem is subjected to a set of constraints as listed below:

• Subject to the power flow equality constraints:

$$f_i^{P^\phi}(x_i, x_{gi}) = P_{g i_{\in \Omega^{\text{Droop}}}}^\phi - P_{di}^\phi - \sum_{\substack{j=1 \\ j \neq i}}^{nbr} \sum_{ph=a,b,c}$$

$$\left[|V_i^\phi||Y_{ij}^{\phi(ph)-n}||V_i^{(ph)}|\cos(\theta_{ij}^{\phi(ph)} + \delta_i^{(ph)} - \delta_i^\phi) \right.$$

$$- |V_i^\phi||Y_{ij}^{\phi(ph)-n}||V_j^{(ph)}|\cos(\theta_{ij}^{\phi(ph)}$$

$$\left. + \delta_j^{(ph)} - \delta_i^\phi) \right] = 0 \qquad \forall_i \forall_\phi \qquad (13)$$

$$f_i^{Q^\phi}(x_i, x_{gi}) = Q_{g i_{\in \Omega^{\text{Droop}}}}^\phi - Q_{di}^\phi - \sum_{\substack{j=1 \\ j \neq i}}^{nbr} \sum_{ph=a,b,c}$$

$$\left[|V_i^\phi||Y_{ij}^{\phi(ph)-n}||V_j^{(ph)}|\sin(\theta_{ij}^{\phi(ph)} + \delta_j^{(ph)} - \delta_i^\phi) \right.$$

$$- |V_i^\phi||Y_{ij}^{\phi(ph)-n}||V_i^{(ph)}|\sin(\theta_{ij}^{\phi(ph)}$$

$$\left. + \delta_i^{(ph)} - \delta_i^\phi) \right] = 0 \qquad \forall_i \forall_\phi \qquad (14)$$

$$V_i^\phi - V_o^\phi + nq_i^\phi Q_{gi}^\phi = 0 \qquad \forall_i \in \Omega_i^{\text{Droop}} \qquad (15)$$

$$d\delta_i^\phi - \omega^* + mp_i^\phi P_{gi}^\phi = 0 \qquad \forall_i \in \Omega_i^{\text{Droop}} \qquad (16)$$

$$V_{i_{\text{ref}}}^{\phi^*} - V_i^{\phi^*} + Z_{v_i} I_{oi}^\phi = 0 \qquad \forall_i \in \Omega_i^{\text{Droop}} \qquad (17)$$

$$|\delta_i^a| - |\delta_i^b| - \frac{2\pi}{3} = 0 \qquad \forall_i \in \Omega_i^{\text{Droop}} \qquad (18)$$

$$|\delta_i^a| - |\delta_i^c| + \frac{2\pi}{3} = 0 \qquad \forall_i \in \Omega_i^{\text{Droop}} \qquad (19)$$

where $f_i^{P^\phi}(x_i, x_{gi})$ and $f_i^{Q^\phi}(x_i, x_{gi})$ are an active and reactive power balance equations for each ith bus and the ϕth phase.

The (x_i, x_{gi}) define the state variables at each ith bus. The θ_{ij} in (13)–(14) is the admittance angle for line (ij) and the δ_i denotes the voltage angle at bus i. The Ω_I^{Droop} defines the group of the droop control buses. The (4), (5), (7) are implemented in the power flow constraints as interpreted in (15)–(17) to model the USPDC-based buses and the USPVIC. For maintaining the phase-shift balance between the three-phase voltage at each droop-based bus, the relations in (18)–(19) are involved in the mismatch equations and are only implemented in the control scheme of Fig. 3 by using the reference voltage generator. The power flow equations and constraints have been solved using the Newton trust region presented in [30].

• The optimization problem is also subjected to additional inequality constraints to set the upper and lower boundaries of the microgrid operation and control parameters, including the system voltage magnitude and angle, system frequency, active and reactive power limits of DERs, and the active and reactive power droop parameters as reported below:

$$V_{i_{\min}}^{\phi} < V_i^{\phi} < V_{i_{\max}}^{\phi} \qquad \forall_{\phi} \forall_i \qquad (20)$$

$$\omega_{\min} < \omega_{o,c} < \omega_{\max} \qquad (21)$$

$$\delta_{i_{\min}}^{\phi} < \delta_i^{\phi} < \delta_{i_{\max}}^{\phi} \qquad \forall_{\phi} \forall_i \qquad (22)$$

$$P_{gi_{\min}}^{\phi} < P_{gi}^{\phi} < P_{gi_{\max}}^{\phi} \qquad \forall_{\phi} \forall_i \in \Omega_i^{\text{Droop}} \qquad (23)$$

$$Q_{gi_{\min}}^{\phi} < Q_{gi}^{\phi} < Q_{gi_{\max}}^{\phi} \qquad \forall_{\phi} \forall_i \in \Omega_i^{\text{Droop}} \qquad (24)$$

$$mp_{i_{\min}}^{\phi} < mp_i^{\phi} < mp_{gi_{\max}}^{\phi} \qquad \forall_{\phi} \forall_i \in \Omega_i^{\text{Droop}} \qquad (25)$$

$$nq_{i_{\min}}^{\phi} < nq_i^{\phi} < nq_{gi_{\max}}^{\phi} \qquad \forall_{\phi} \forall_i \in \Omega_i^{\text{Droop}}. \qquad (26)$$

It is noteworthy that the values of the upper and lower boundaries for the UBIMG operation and control parameters defined in (20)–(26) are set to ensure that the obtained USPDVIC settings maintain the operation of the UBIMG within the desired operation limits. For example, the boundaries of the voltage magnitudes and system frequency, defined in (20) and (21), respectively, are set based on the applicable standards IEEE Std 1547–2003 for voltage and frequency operation limits [24]. Also, the boundaries of the droop parameters defined in (25) and (26) are chosen to ensure that the corresponding parameters of the frequency and voltage references degrade by less than 1% of their rated nominal values under the rated loading conditions that guarantee the stability of the microgrid [31], [32].

To optimize the objective functions in (10) and (12) concurrently, the competitive multiobjective cooperative swarm optimizer (CMOCSO) [33] is tailored and combined with the power flow equations [30]. The CMOCSO was selected as it proved its efficiency in solving large-scale multiobjective optimization problems using IEEE CEC 2021. In CMOCSO, the two objective functions are evaluated concurrently, and the obtained solutions are sorted and clustered into dominated and nondominated (ND) solutions. The Pareto approach displays a set of feasible (non-dominated) solutions stored in the archive [33]. However, only one solution is recommended from the Pareto front as the final solution to the optimized multiobjectives (Obj_1, Obj_2), known

as the best compromise solution (BCS). The fuzzy decision-making (FDM) was a widely conducted strategy in defining the BCS where the fuzzy membership approach normalizes the optimized values of the objective functions (Obj_1, Obj_2) in (10) and (12) of each NDth solutions between 0 and 1 as expressed below:

$$\mu_{(1,2)}^{ND}$$

$$= \begin{cases} 1 & Obj_{(1,2)} < Obj_{(1,2)_{\min}} \\ \frac{Obj_{(1,2)_{\max}} - Obj_{(1,2)}}{Obj_{(1,2)_{\max}} - Obj_{(1,2)_{\min}}} & Obj_{(1,2)_{\min}} < Obj_{(1,2)} < Obj_{(1,2)_{\max}} \\ 0 & Obj_{(1,2)} > Obj_{(1,2)_{\max}} \end{cases}$$

$$(27)$$

where $Obj_{(1,2)_{\min}}$ and $Obj_{(1,2)_{\max}}$ are the minimum and maximum values of the objective functions (Obj_1, Obj_2) in (10) and (12) corresponding to the NDth solution. The $\mu_{(1,2)}^{ND}$ is the fuzzy-membership function of the two objective functions in (10) and (12). The normalized membership function μ^{ND} as in (28) is then computed to determine the BCS where the recommended solution corresponds to the larger membership function

$$\mu^{ND} = \frac{\mu_1^{ND} + \mu_2^{ND}}{\sum_{ND}^{L} \left(\mu_1^{ND} + \mu_2^{ND} \right)} \qquad (28)$$

where L is the length of the ND solutions. The flowchart in Fig. 4 outlines the primary steps involved in concurrently solving the objective functions to determine the BCS from the Pareto front for the USPDVIC settings across M sets of operating states.

V. CASE STUDIES AND ANALYSIS

This section presents an extensive assessment of the proposed USPDVIC and the optimization process of Section IV performance in enhancing RPS throughout a set of operating states in different systems. The systems analyzed include a parallel architecture UBIMG with two connected dispatchable DERs of Fig. 1 and radial UBIMGs-based IEEE 13-bus, IEEE 34-bus, and IEEE 123-bus benchmark systems of Fig. 5(a), (b), and (c), respectively [34]. As shown in the figure, there are 3, 5, and 6 dispatchable DERs, respectively.

A. Investigate the Proposed USPDVIC in RPS Within Parallel Architecture UBIMG

In this part, the performance of the proposed USPDVIC is evaluated using the UBIMG of Fig. 1. in the context of heterogeneous line impedances $(Z_2^{\phi} > Z_1^{\phi})$ under two case studies: (C1) the two DERs have the same capacities, and (C2) the capacity of DER$_2$ is double the capacity of DER$_1$. Both cases include two states of loading condition: the first state (St1) occurs when $t < 1.5$ s with an unbalanced three-phase load of $((5, 2, 7)\text{kW}, (0.5, 0.9, 1.1) \text{kVAR})$, and the second loading state (St2) begins at $t > 1.5$ s when an unbalanced load of $((1, 2, 1)\text{kW}, (0.5, 1, 0.0001)\text{kVAR})$ is connected.

For comparison with the literature, the studied cases incorporate four control schemes from the literature: TDC [35], VCC, as devised in [15], AVIC as detailed in [16], and the SPDC discussed in [22]. In addition, symmetrical per-phase droop control coupled with a symmetrical virtual impedance control
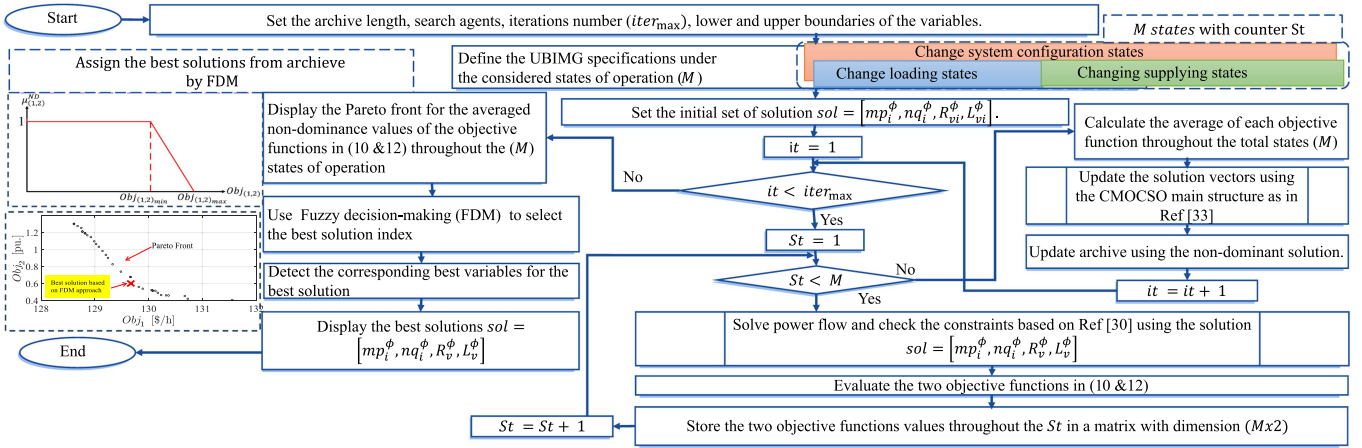
This article has been accepted for inclusion in a future issue of this journal. Content is final as presented, with the exception of pagination.

8   IEEE TRANSACTIONS ON INDUSTRIAL INFORMATICS

Fig. 4.   Flowchart of main steps while identifying a unified set of USPDVIC settings fit M operating states.
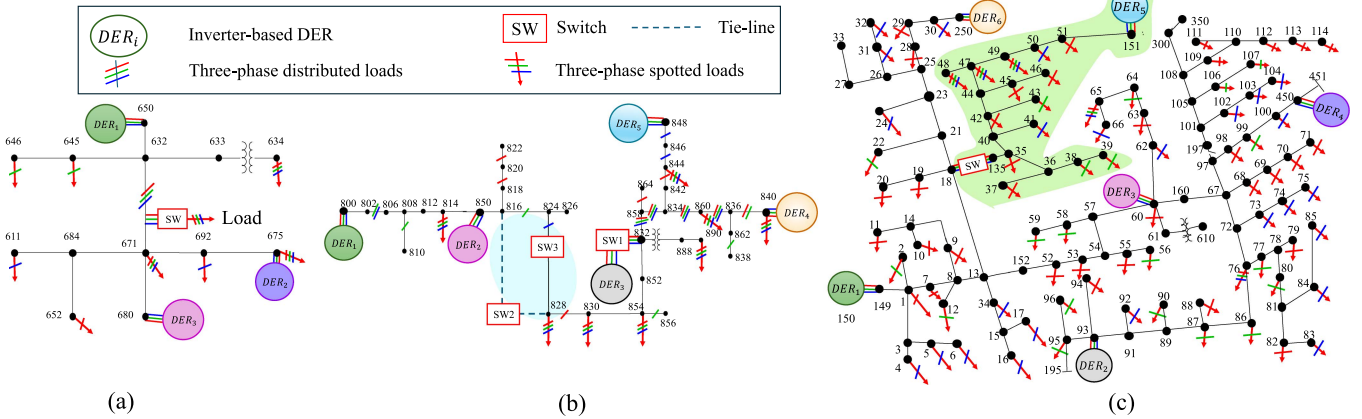

Fig. 5.   UBIMG-based (a) IEEE-13 bus, (b) IEEE-34 bus, and (c) IEEE-123 bus benchmark systems [34] with 3, 5, and 6 dispatchable DERs, respectively.

TABLE I
SETTINGS AND SPECIFICATIONS OF THE IMPLEMENTED CONTROLLERS AND TWO-DERS PARALLEL ARCHITECTURE UBIMG OF FIG. 1

Item	Symbol	Value
Nominal voltage (L-L)	V_{n_i}	381.05 (V).
Nominal frequency	ω_{ni}	376.9911 (rad/s).
Filter inductor	L_f	1.35 (mH).
Filter capacitor	C_f	0.5 (μF).
Filter resistor	R_f	0.1 (Ω).
line (1,2) impedance (C1,2)	$r1,2,L1,2$	0.03, 0.27 (Ω), 0.35, 0.7389 (mH)
TDC. droop coefficients (C1) [35]	$m_{1,2}, n_{1,2}$	$6.150e^{-5}, 1.65e^{-3}$
TDC. droop coefficients (C2) [35]	$m_{1,2}, n_{1,2}$	$(1.230e^{-4}, 6.150e^{-5}), (3.30e^{-3}, 1.65e^{-3})$
AVIC. droop coefficients (C1) [16]	$m_{1,2}, n_{1,2}$	$6.150e^{-5}, 1.65e^{-3}$
AVIC. droop coefficients (C2) [16]	$m_{1,2}, n_{1,2}$	$(1.230e^{-4}, 6.150e^{-5}), (3.30e^{-3}, 1.65e^{-3})$
AVIC. adaptive coefficients (C1,2) [16]	R_V, x, L_V, y	$0.0325(\Omega), 0.01, 0.314(mH), 1e^{-3}$
VCC. droop coefficient (C1,2) [15]	$n_{c1,2}$	0.7391, 0.7410
SPD. droop coefficients (C1) [22]	$m^{\phi}_{1,2}, n^{\phi}_{1,2}$	$6.769e^{-5}, 6.016e^{-3}$
SPD. droop coefficients (C2) [22]	$m^{\phi}_{1,2}, n^{\phi}_{1,2}$	$(1.354e^{-4}, 6.769e^{-5}), (1.2036e^{-2}, 6.016e^{-3})$
SPDVI. per-phase VIC (C1,2)	R^{ϕ}_V, L_V	2.701, 6.032(m H)
Unbalanced load	$P^{\phi \in (a,b,c)}, Q^{\phi \in (a,b,c)}$	((5,2,7) kW, (0.5,0.9,1.1) kVAR) of st1 at $t \le 1.5$ then ((1,2,1) kW, (0.5,1,0.0001) kVAR) of st2 at $t > 1.5$.
Base power	S	1.5 MVA.

scheme (SPDVIC) is developed and examined in the studied cases to provide a broad evaluation of the performance of the proposed USPDVIC versus the symmetrical-based control schemes in RPS within the UBIMG. The UBIMG specifications and control parameters of TDC, VCC, AVIC, SPDC, and SPDVIC are outlined in Table I. The unique identified USPDVIC settings using the optimization process in Section IV are listed in Table II.

TABLE II
IDENTIFIED USPDVIC WITHIN TWO-DERS PARALLEL ARCHITECTURE UBIMG OF FIG. 1

	DER_{g1}				DER_{g2}		
	Phase a	Phase b	Phase c		Phase a	Phase b	Phase c
mp^{ϕ}_1	5.971×10^{-5}	4.969×10^{-5}	6.221×10^{-5}	mp^{ϕ}_2	5.725×10^{-5}	4.886×10^{-5}	6.205×10^{-5}
nq^{ϕ}_1	2.586×10^{-2}	1.671×10^{-2}	6.221×10^{-2}	nq^{ϕ}_2	1.713×10^{-2}	1.179×10^{-2}	1.560×10^{-2}
$R^{\phi}_{v1}(\Omega)$	0.0161	0.0873	0.0076	$R^{\phi}_{v2}(\Omega)$	2.5816	0.1334	2.5645
$L^{\phi}_{v1}(mH)$	5.3501	3.0511	1.0302	$L^{\phi}_{v2}(mH)$	3.5491	7.2012	6.9280

The details of the analysis and comparisons are reported in the following sections:

1) Analysis of the Proposed USPDVIC Controller: To comprehensively analyze the proposed USPDVIC controller and the identified settings in Table II, the per-phase reactive power profiles generated by the parallel-connected DERs-based US-PDVIC are presented in Fig. 6 for C1 and C2.

Fig. 6(a) displays the sharing of per-phase reactive power among the DERs accomplished with C1. During the St1, the total unbalanced reactive power of (0.5, 0.9, and 1.1) kVAR is uniformly dispatched per-phase across the two identical DERs. Consequently, the desired per-phase sharing is (0.25, 0.45, and 0.55) $\times 10^{-3}$ pu. Concerning Fig. 6(a), the dispatched reactive
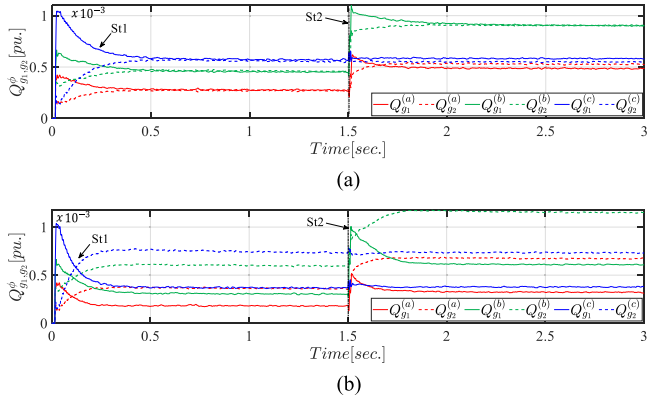
Fig. 6. Per-phase RPS profiles by the proposed USPDVIC under heterogeneous line impedance within changes in unbalanced loading condition in cases of (a) C1: identical DERs, and (b) C2: unequal DERs capacities (DER$_2$ = 2 DER$_1$) within two-DERs parallel architecture UBIMG of Fig. 1.
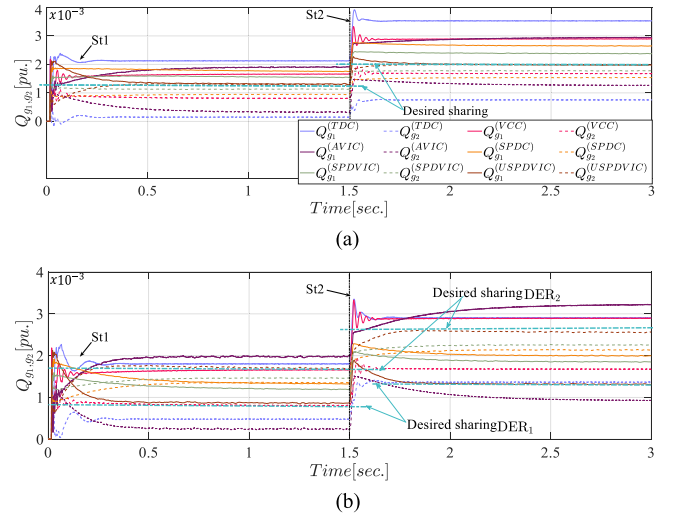

Fig. 7. RPS profiles by the proposed USPDVIC versus previously published controllers under heterogeneous line impedance within changes in unbalanced loading condition in cases of (a) identical DERs, and (b) unequal DERs capacities (DER$_2$= 2 DER$_1$) within parallel architecture UBIMG of Fig. 1.

power from phases "a, b, c" of DER$_1$ and DER$_2$ are found to be (0.277, 0.459, 0.561) $\times 10^{-3}$ pu and (0.270, 0.456, 0.571) $\times 10^{-3}$ pu, respectively. The observed dispatched per-phase reactive power vividly demonstrates the efficiency of the proposed approach in nearly achieving an equal sharing of unbalanced per-phase reactive power among the phases of the two DERs. Moving on to the St2, the degree of imbalance escalates by connecting an unbalanced three-phase load characterized by magnitudes of (0.5, 1, 0.0001) kVAR. Upon scrutinizing the per-phase RPS in Fig. 6(a), it becomes evident that the proposed methodology yields a highly accurate sharing for the load associated with phases as observed in phase "b" of DERs.

In C2, the capacities of DER$_2$ is twice that of DER$_1$, consequently, DER$_2$ provides per-phase reactive power that is twice that of DER$_1$. Referring to Fig. 6(b), during st1 loading state ($t < 1.5$), DER$_1$ supplies (0.179, 0.304, 0.366) $\times 10^{-3}$ pu, while DER$_2$ delivers (0.363, 0.600, 0.743) $\times 10^{-3}$ pu to meet the demand of (0.5, 0.9, and 1.1) $\times 10^{-3}$ pu. In the subsequent loading phase, with a total per-phase reactive power demand of (1, 1.9, 1.1001) $\times 10^{-3}$ pu because of connecting the unbalanced load of (0.5, 1, 0.0001) $\times 10^{-3}$ pu at $t > 1.5$, DER$_1$ provides (0.323, 0.616, 0.372) $\times 10^{-3}$ pu, while DER$_2$ contributes (0.6773, 1.1565, 0.7398) $\times 10^{-3}$ pu. The dispatched reactive power throughout these two loading phases confirms the ability of the proposed controller to achieve proportional RPS among the DER capacities, with DER$_2$'s capacity being nearly double that of DER$_1$. This demonstrates its efficiency in addressing challenges such as heterogeneity in the line impedance, load imbalances, and unequal DER capacities.

2) Comprehensive Comparison With the Literature: To demonstrate the response of the proposed USPDVIC and the identified settings in Table II, in comparison to the literature models, including TDC [35], VCC [15], AVIC [16], SPDC [22], and SPDVIC, Fig. 7 depicts the aggregated three-phase reactive power shared across the studied cases to achieve the desired RPS among the connected DERs.

In the context of C1, attaining equitable RPS of 1.25×10^{-3} pu at St1 and 2×10^{-3} pu at St2 among the parallel-connected DERs of UBIMG of Fig. 1 within the heterogeneity in the line impedance ($Z_2^\phi > Z_1^\phi$) and an unbalanced load presents a notable challenge. Fig. 7(a) visually represents RPS among the two DERs using various control strategies, including TDC, VCC, AVIC, SPDC, and SPDVIC versus USPDVIC. The figure clearly illustrates that TDC exhibits the worst performance, displaying a notable deviation from the desired RPS values. The DER$_1$, which employs TDC, experiences an overload, contributing the largest share of reactive power, namely, 2.126 $\times 10^{-3}$ pu at St1 and 3.519 $\times 10^{-3}$ pu at St2. This underscores TDC's inability to cope with the challenges posed by the heterogeneity in line impedance ($Z_2^\phi > Z_1^\phi$). Connecting symmetric virtual impedance/capacitance with TDC, as in AVIC and VCC, shows marginal improvements to the RPS compared to the TDC. Implementing the SPDC also results in limited improvement in RPS as the DER$_1$ becomes overloaded, contributing 1.77 $\times 10^{-3}$ pu at St1 and 2.67 $\times 10^{-3}$ pu at St2, whereas the desired sharing is 1.25 $\times 10^{-3}$ pu at St1 and 2 $\times 10^{-3}$ pu at St2, respectively. Integrating the symmetric virtual impedance and symmetric per-phase droop control as in SPDVIC shows better response than using solo SPDC, yet remarkable overloading for DER$_1$ is still detected as the shared reactive power are 1.55 $\times 10^{-3}$ pu and 2.40 $\times 10^{-3}$ pu over st1 and st2, respectively. Implementing the USPDVIC shows a significant enhancement to the RPS compared to the other conducted control schemes, as the DERs almost share the same reactive power over st1 and st2.

In the context of C2 of analysis, the capacity of the DER$_2$ is twice that of DER$_1$. Accordingly, the control scheme settings outlined in Tables I and II for DER$_1$ are multiplied by 2. Considering the capabilities of the DERs, the desired RPS targets by (DER$_1$, DER$_2$) are (0.833, 1.667) $\times 10^{-3}$ pu and (1.334, 2.667)

This article has been accepted for inclusion in a future issue of this journal. Content is final as presented, with the exception of pagination.

10

IEEE TRANSACTIONS ON INDUSTRIAL INFORMATICS

		$\%e_{(Q_{gi})} : TDC$	$\%e_{(Q_{gi})} : VCC$	$\%e_{(Q_{gi})} : AVIC$	$\%e_{(Q_{gi})} : SPDC$	$\%e_{(Q_{gi})} : SPDVIC$	$\%e_{(Q_{gi})} : $ **USPDVIC**
		St1 $t < 1.5$ s					
C1	DER_1	70.08	32.65	51.74	41.60	24.00	**3.76**
	DER_2	88.51	35.04	74.10	24.32	9.06	**3.76**
		St2 $t > 1.5$ s					
C1	DER_1	75.95	45.45	45.97	32.75	20.00	**0.1**
	DER_2	62.90	15.90	35.00	23.44	11.00	**0.1**
		St1 $t < 1.5$ s					
C2	DER_1	117.28	97.30	138.36	62.44	45.66	**1.92**
	DER_2	71.53	51.36	85.02	18.64	12.06	**2.33**
		St2 $t > 1.5$ s					
C2	DER_1	117.59	117.38	140.36	50.69	39.16	**1.72**
	DER_2	48.59	37.23	62.89	19.87	15.57	**3.50**

$\times 10^{-3}$ pu over st1 and st2, respectively. Fig. 7(b) visually represents the reactive power dispatched by the parallel-connected DERs, employing various control strategies, including TDC, VCC, AVIC, SPDC, and SPDVIC versus USPDVIC. Fig. 7(b) demonstrates that TDC, VCC, AVIC, SPDC, and SPDVIC struggle to address this case, with a significant deviation from the desired sharing observed. The implementation of USPDVIC yields a remarkable response as the DER_1 contributes (0.849, 1.311) $\times 10^{-3}$ pu, and DER_2 participates by (1.706, 2.5736) $\times 10^{-3}$ pu over st1 and st2, respectively.

To quantitatively evaluate the effectiveness of the USPDVIC in terms of RPS versus TDC, VCC, AVIC, SPDC, and SPDVIC, the percentage of RPS error between the desired shared reactive power (Q_{des}) and the measured Q_{gi} at the ith DER terminal is computed using the subsequent relationship and presented in Table III

$$\%e_{(Q_{gi})} = \frac{|Q_{gi} - Q_{des}|}{Q_{des}} \times 100. \quad (29)$$

The reported data in Table III affirm the significant improvement that the USPDVIC scheme provides in minimizing errors in RPS of the parallel-connected DERs compared to the other implemented controllers; that improvement is instrumental in mitigating the adverse effects of RPS mismatches. The key feature contributing to this success of USPDVIC lies in the ability to address the imbalance of the power flow in each phase and heterogeneity in per-phase line impedance.

B. Investigate the Proposed USPDVIC in RPS Within Radial UBIMG

In this part, the performance of the proposed controller is investigated using the three radial benchmark distribution systems of Fig. 5 to assess the controller's response across a range of scalable and varied configuration systems.

1) Analysis of the Proposed USPDVIC Within IEEE-13 Bus: The effectiveness of the proposed USPDVIC is specifically analyzed within a radial UBIMG based on the IEEE-13 bus benchmark system [34]. The microgrid includes three identical dispatchable DERs, each rated at 1.5 MVA, as depicted in Fig. 5(a). The controller parameters, obtained by optimizing the objective functions (10) and (12) using CMOCSO, are detailed in Table IV. The USPDVIC and its identified settings are subjected to testing under various loading states. The evaluation includes default loading conditions until $t = 3$ s, followed by the introduction of an additional unbalanced three-phase load

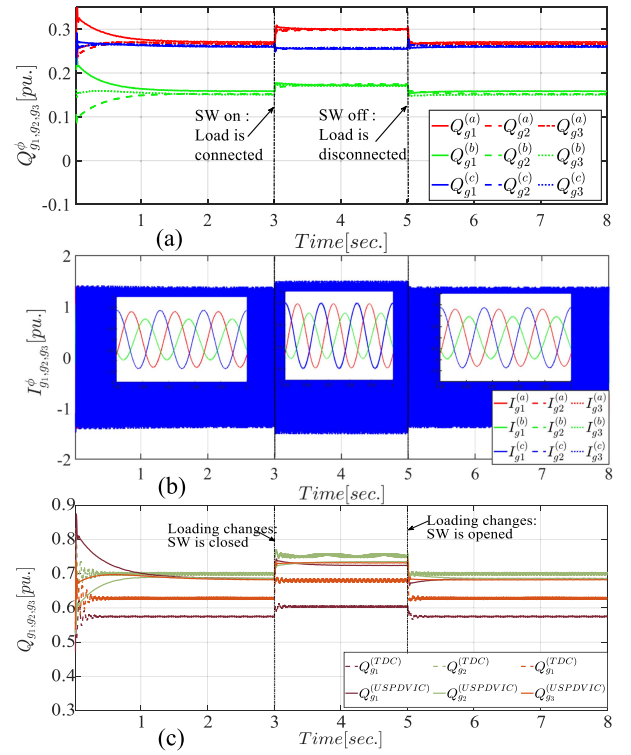		\multicolumn{3}{c}{DER_1}				\multicolumn{3}{c}{DER_2}		
	Phase a	Phase b	Phase c		Phase a	Phase b	Phase c
mp_1^ϕ	1.0011×10^{-6}	1.4920×10^{-6}	1.7578×10^{-6}	mp_2^ϕ	3.4723×10^{-6}	1.8252×10^{-6}	2.4308×10^{-6}
nq_1^ϕ	3.5931×10^{-4}	4.9611×10^{-4}	1.6347×10^{-4}	nq_2^ϕ	3.1259×10^{-4}	4.9444×10^{-5}	2.4470×10^{-4}
$R_{c1}^\phi(\Omega)$	15.5157	3.9898	8.3745	$R_{c2}^\phi(\Omega)$	0.0810	2.0155	0.5211
$L_{c1}^\phi(mH)$	3.014	3.42	0.458	$L_{c2}^\phi(mH)$	1.486	2.190	2.583
	DER_3					
mp_3^ϕ	2.0265×10^{-6}	1.0132×10^{-6}	1.9727×10^{-6}	nq_3^ϕ	3.0439×10^{-4}	2.2709×10^{-4}	2.1217×10^{-4}
$R_{c3}^\phi(\Omega)$	4.5130	5.7068	2.7096	$L_{c3}^\phi(mH)$	1.759	3.359	2.496

Fig. 8. Proposed USPDVIC performance using (a) per-phase reactive power, (b) per-phase generated DERs' currents, and (c) three-phase reactive power versus TDC within a radial IEEE-13 bus UBIMG.

of (100, 50, 200) kW and (30, 20, 5) kVAR connected through the closing of a switch (SW) in Fig. 5(a). At $t = 5$ s, the SW is reopened, resulting in the disconnection of the additional load. To comprehensively evaluate the performance of the proposed USPDVIC method based on the unique identified settings, the per-phase reactive power and per-phase currents of the DERs are monitored, as depicted in Fig. 8(a) and (b). In addition, US-PDVIC is compared with TDC using the aggregated three-phase RPS, as visualized in Fig. 8(c).

The plotted profiles of per-phase RPS among the three connected DERs in Fig. 8(a) affirm the effectiveness of employing the unsymmetrical approach and the unique identified settings in managing power flow in each phase almost independently. Throughout the simulation time, each phase of the connected DERs equally contributes to meeting the required demand for its corresponding phase. For instance, during the default loading at $t < 3$ s and $t > 5$ s, where the phases "a, b, c" of the simulated IEEE-13 bus system requires a total per-phase reactive power about (0.8341, 0.4568, and 0.8203) pu, respectively, the per-phase RPS in Fig. 8(a) indicates that each of the three DERs

TABLE V
IDENTIFIED USPDVIC WITHIN RADIAL IEEE-34 BUS UBIMG

|	DER₁				DER₂		
	Phase a	Phase b	Phase c		Phase a	Phase b	Phase c
mp_{g1}^ϕ	2.106×10^{-4}	1.117×10^{-4}	1.766×10^{-4}	mp_{g2}^ϕ	3.186×10^{-4}	4.999×10^{-4}	3.588×10^{-4}
nq_{g1}^ϕ	2.132×10^{-2}	3.074×10^{-2}	2.405×10^{-2}	nq_{g2}^ϕ	3.120×10^{-2}	2.955×10^{-2}	2.303×10^{-2}
$R_{v1}^\phi(\Omega)$	657.57	895.56	967.12	$R_{v2}^\phi(\Omega)$	254.43	431.17	674.37
$L_{v1}^\phi(H)$	-0.3875	-0.3931	-1.1557	$L_{v2}^\phi(H)$	0.1737	0.6970	0.0200
	DER₃				DER₄		
mp_{g3}^ϕ	2.013×10^{-4}	1.797×10^{-4}	2.718×10^{-4}	mp_{g4}^ϕ	2.538×10^{-4}	2.159×10^{-4}	3.353×10^{-4}
nq_{g3}^ϕ	3.150×10^{-2}	5.253×10^{-2}	3.497×10^{-2}	nq_{g4}^ϕ	3.317×10^{-2}	4.251×10^{-2}	2.445×10^{-2}
$R_{v3}^\phi(\Omega)$	0.1096	0.0579	1.5447	$R_{v4}^\phi(\Omega)$	0.2185	4.9310	3.0894
$L_{v3}^\phi(H)$	0.0984	0.0498	0.8354	$L_{v4}^\phi(H)$	0.0635	0.1562	1.3560
	DER₅						
mp_{g5}^ϕ	4.459×10^{-4}	2.548×10^{-4}	2.578×10^{-4}	nq_{g5}^ϕ	3.612×10^{-2}	4.052×10^{-2}	4.237×10^{-2}
$R_{v5}^\phi(\Omega)$	1.1510	1.3764	4.6965	$L_{v5}^\phi(H)$	0.1214	0.2967	0.6578

Fig. 9. Proposed USPDVIC performance using (a) per-phase reactive power, (b) per-phase generated DERs' currents, and (c) three-phase reactive power versus TDC within a radial IEEE-34 bus UBIMG.

contributes by (0.2773, 0.1527, and 0.2701) pu for phases "a, b, c," respectively. This RPS ensures that each phase supplies the required demand without overloading, thereby helping to avoid circulating reactive power issues. During the closing of the SW ($3 < t < 5$ s), leading to the connection of an unbalanced three-phase load of (30, 20, 5) kVAR (the loading of phase "a"> "b"> "c"), Fig. 8(a) illustrates a notable increase in RPS in phase "a" compared to phase "b," while, phase "c" shows minimal change as a small load is connected to it. This observation confirms the ability of the proposed control scheme to handle RPS by each phase almost separately. Furthermore, the generated per-phase current in Fig. 8(b) provides evidence of the efficiency of the proposed control scheme and the unique identified settings in addressing the impact of the heterogeneity of the feeder impedance in the IEEE-13 bus system as the three DERs almost generate identical per-phase current levels before and after changing the loading condition.

For comparison, the aggregated RPS by the DERs based on the proposed USPDVIC and TDC are plotted in Fig. 8(c). The depicted profiles highlight the deficiency of TDC in handling RPS under the presence of feeder impedance heterogeneity and unbalanced loads. In contrast, the DERs' RPS based on the proposed USPDVIC illustrates the superiority of this approach in achieving almost equal RPS. This observation emphasizes the efficiency of implementing the unsymmetrical approach to address challenges associated with feeder impedance heterogeneity and unbalanced loads.

2) Analysis of the Proposed USPDVIC Within IEEE-34 Bus: In this part of analysis, the proposed USPDVIC controller performance is investigated under a larger scale system with different DER arrangements compared with the investigated system in Section V-B1. The considered system in this part is a radial UBIMG based on the IEEE-34 bus benchmark system in [34] with five identical DERs rated equally at 0.75 MVA, as depicted in Fig. 5(b). The unique identified controller parameters based on optimizing the objective functions in (10) and (12) using CMOCSO are reported in Table V. The proposed USPDVIC and identified settings are tested under a set of operating states, including default loading and configuration setup of IEEE-34 UBIMG as in [34], plug-and-play capability, and change the system reconfiguration.

The UBIMG-based IEEE-34 bus system of Fig. 5(b) operates under the default loading condition and configuration as in [34] from $t = 0$ s to $t = 4$ s; hence the simulated model requires a total per-phase reactive power about (0.2303, 0.110, and 0.035)
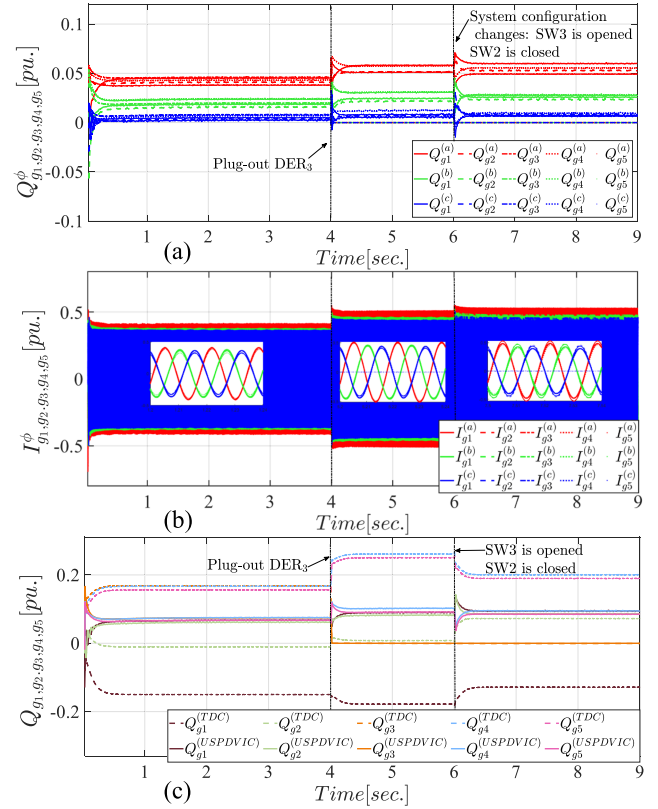
pu. At $t = 4$ s, the circuit breaker (SW1), as indicated in Fig. 5(b), for DER₃ is opened. Subsequently, at $t = 6$ s, a system reconfiguration change is introduced through the closure of SW2 and the opening of SW3, as illustrated in Fig. 5(b). To evaluate the performance of the proposed USPDVIC based on the unique identified settings comprehensively, the per-phase RPS and the per-phase generated currents of the DERs are monitored, as depicted in Fig. 9(a) and (b). Furthermore, the aggregated DER RPS are tracked in comparison to that of the DERs based on the TDC controller as visualized in Fig. 9(c).

Fig. 9(a) demonstrates the reliability of the unsymmetrical proposed approach in achieving nearly equal per-phase RPS among the five connected DERs where each DER nearly shares by (0.0461, 0.0367, and 0.0069) pu during the default setup period ($0 < t < 4$ s). This is notable even with the features of the IEEE-34 bus-based UBIMG, where the line impedance is mismatched, and unbalanced three-phase and single-phase connections are involved. When DER₃ is disconnected ($4 < t$), the proposed USPDVIC ensures a fair allocation of required RPS among the other four DERs with minimal deviation in sharing, as illustrated in Fig. 9(a). During the system reconfiguration process at $t = 6$ s, the proposed approach exhibits a remarkable response in achieving nearly identical RPS among the four interconnected DERs within the UBIMG, as in Fig. 9(a). Furthermore, the per-phase current profiles in Fig. 9(b) affirm the efficiency of the proposed USPDVIC in the three sequential

This article has been accepted for inclusion in a future issue of this journal. Content is final as presented, with the exception of pagination.

12   IEEE TRANSACTIONS ON INDUSTRIAL INFORMATICS

TABLE VI
IDENTIFIED USPDVIC WITHIN RADIAL IEEE-123 BUS UBIMG

|	DER₁				DER₂		
	Phase a	Phase b	Phase c		Phase a	Phase b	Phase c
mp_1^ϕ	3.3340×10^{-5}	2.8776×10^{-5}	3.4735×10^{-5}	mp_2^ϕ	3.0461×10^{-5}	4.6505×10^{-5}	1.5662×10^{-5}
nq_1^ϕ	2.1113×10^{-4}	1.5920×10^{-4}	1.1578×10^{-4}	nq_2^ϕ	1.1235×10^{-4}	4.9844×10^{-4}	1.2755×10^{-4}
$R_{v1}^\phi(\Omega)$	0.0812	0.4656	0.1375	$R_{v2}^\phi(\Omega)$	0.6516	0.0828	0.2752
$L_{v1}^\phi(H)$	0.0339	0.0354	0.0428	$L_{v2}^\phi(H)$	0.0241	0.0111	0.0156
	DER₃				DER₄		
	Phase a	Phase b	Phase c		Phase a	Phase b	Phase c
mp_3^ϕ	6.3960×10^{-5}	3.8349×10^{-5}	2.9329×10^{-5}	mp_4^ϕ	4.9862×10^{-6}	6.8772×10^{-6}	5.8570×10^{-6}
nq_3^ϕ	1.0978×10^{-4}	8.8704×10^{-4}	1.1007×10^{-4}	nq_4^ϕ	3.1254×10^{-4}	2.7525×10^{-4}	1.6347×10^{-4}
$R_{v3}^\phi(\Omega)$	2.0176	1.6750	1.4118	$R_{v4}^\phi(\Omega)$	1.6018	1.0063	0.8326
$L_{v3}^\phi(H)$	0.0319	0.0299	0.0368	$L_{v4}^\phi(H)$	0.0255	0.0236	0.0266
	DER₅				DER₆		
	Phase a	Phase b	Phase c		Phase a	Phase b	Phase c
mp_5^ϕ	5.9891×10^{-6}	4.5001×10^{-5}	7.6707×10^{-5}	mp_6^ϕ	1.0891×10^{-5}	3.5201×10^{-5}	1.7907×10^{-5}
nq_5^ϕ	1.9672×10^{-4}	2.0417×10^{-4}	3.0018×10^{-4}	nq_6^ϕ	6.7270×10^{-4}	7.8704×10^{-4}	6.4245×10^{-4}
$R_{v5}^\phi(\Omega)$	0.8701	0.7388	0.9853	$R_{v6}^\phi(\Omega)$	1.1110	1.5124	1.1313
$L_{v5}^\phi(H)$	0.0469	0.0459	0.0424	$L_{v6}^\phi(H)$	0.0378	0.0363	0.0519

Fig. 10. Proposed USPDVIC performance using (a) per-phase reactive power, and (b) three-phase reactive power versus TDC within a radial IEEE-123 bus UBIMG.

operating states, where all the five DERs generate almost identical per-phase current levels during the default setup period of $0 < t < 4$ s. When DER₃ is disconnected $(4 < t)$, the per-phase current levels of the four interconnected DERs increase by nearly the same levels to compensate. After the system reconfiguration changes, the four connected DERs share almost identical per-phase current levels, as shown in Fig. 9(b).

In the comparison stage, Fig. 9(c) shows the superiority of employing the unsymmetrical approach to address challenges associated with feeder impedance heterogeneity and unbalanced loads versus implementing the TDC. This response is attributed to the effectiveness of the unsymmetrical per-phase approach in addressing the impacts of line impedance mismatch and imbalance loads for each phase individually.

3) Analysis of the Proposed USPDVIC Within IEEE-123 Bus: For the purpose of increasing the complexity of the tested system and assessing the generality of the proposed controller and the unique identified settings of Table VI based on the optimization process of Section IV, the IEEE-123 benchmark system of Fig. 5(c) is considered in this part of the validation. The considered cases include operation under the default configuration with six dispatchable DERs and then partitioning the system into two separate UBIMG at $t = 1$ s followed by recombining the two UBIMG at $t = 2$ s. To evaluate the proposed controller based on the unique control settings' performance, the per-phase RPS among the connected six dispatchable DERs is depicted in Fig. 10(a), and the aggregated PRS is visualized in Fig. 10(b) for both the TDC and the proposed controller.

Fig. 10(a) illustrates that the proposed unsymmetrical approach based on the identified parameters in Table VI achieves nearly identical per-phase RPS among the connected six dispatchable DERs within the large-scale IEEE-123 benchmark system without communication. In the case of partitioning the system into separate UBIMGs, UBIMG includes DERs₁,₂,₃,₄,₆, and the other one has DER₅. The per-phase RPS profiles of DERs₁,₂,₃,₄,₆, based on the proposed approach, show identical RPS, especially in phases "a" and "c." The aggregated RPS by the proposed approach versus the TDC in Fig. 10(b) highlights the superiority of the proposed approach in enhancing the RPS among the DERs in a large scale and complex system like the IEEE-123 benchmark. This comparison provides further evidence of the effectiveness of the proposed unsymmetrical approach in managing power flow variations across phases and
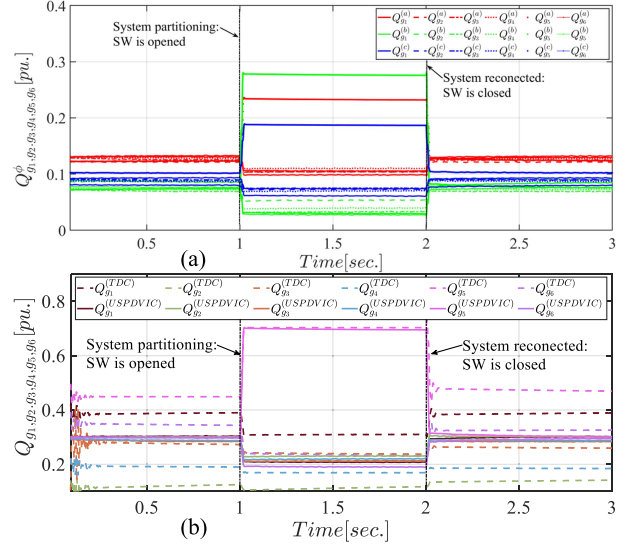
line impedance heterogeneity within the UBIMG, even in the absence of communication.

VI. CONCLUSION

To address the challenges stemming from imprecise RPS within UBIMG, this article introduces an advanced solution: the unsymmetrical per-phase-based control scheme. This proposed approach effectively tackles issues related to line impedance mismatches and load imbalances. The proposed USPDVIC scheme is designed to enhance the sharing of RPS among DERs within the UBIMG. To ensure the cost-effective operation of UBIMG across various operating scenarios without the need for frequent communication, a unique set of control settings for the proposed controller has been identified. This identification is accomplished through a multiobjective optimization approach that simultaneously minimizes average generation costs while reducing average deviations in per-phase RPS within the UBIMG across a predefined set of operational states. The performance of the USPDVIC scheme is comprehensively evaluated for both a parallel architecture UBIMG and radial UBIMG-based IEEE 13-bus, IEEE 34-bus, and IEEE 123-bus benchmark systems. These evaluations span a range of operational states, encompassing changes in loading conditions, plug-and-play capability, and system reconfiguration and partitioning processes. The effectiveness of the proposed approach is rigorously tested against various controller schemes presented in the literature. The results, coupled with comparisons to existing research, provide compelling evidence for the efficiency of implementing the USPDVIC control scheme to enhance the RPS among interconnected dispatchable DERs within the UBIMG proportionate to their capacities. This improvement is instrumental in mitigating the adverse effects of RPS mismatches and ensuring a more resilient and efficient operation of UBIMGs.

This article has been accepted for inclusion in a future issue of this journal. Content is final as presented, with the exception of pagination.

YOUSRI et al.: UNSYMMETRICAL PER-PHASE CONTROL FOR REACTIVE POWER-SHARING ENHANCEMENT 13

REFERENCES

[1] R. An, J. Liu, Z. Liu, and Z. Song, "Flexible transfer converters enabling autonomous control and power dispatch of microgrids," *IEEE Trans. Power Electron.*, vol. 37, no. 11, pp. 13767–13781, Nov. 2022.

[2] N. Mohammed, A. Lashab, M. Ciobotaru, and J. M. Guerrero, "Accurate reactive power sharing strategy for droop-based islanded AC microgrids," *IEEE Trans. Ind. Electron.*, vol. 70, no. 3, pp. 2696–2707, Mar. 2023.

[3] M. Minetti, A. Rosini, G. B. Denegri, A. Bonfiglio, and R. Procopio, "An advanced droop control strategy for reactive power assessment in islanded microgrids," *IEEE Trans. Power Syst.*, vol. 37, no. 4, pp. 3014–3025, Jul. 2021.

[4] B. Liu, Z. Liu, J. Liu, R. An, H. Zheng, and Y. Shi, "An adaptive virtual impedance control scheme based on small-AC-signal injection for unbalanced and harmonic power sharing in islanded microgrids," *IEEE Trans. Power Electron.*, vol. 34, no. 12, pp. 12333–12355, Dec. 2019.

[5] Y. C. C. Wong, C. S. Lim, M. D. Rotaru, A. Cruden, and X. Kong, "Consensus virtual output impedance control based on the novel droop equivalent impedance concept for a multi-bus radial microgrid," *IEEE Trans. Energy Convers.*, vol. 35, no. 2, pp. 1078–1087, Jun. 2020.

[6] M. Chen, X. Xiao, and J. M. Guerrero, "Secondary restoration control of islanded microgrids with a decentralized event-triggered strategy," *IEEE Trans. Ind. Inform.*, vol. 14, no. 9, pp. 3870–3880, Sep. 2018.

[7] L. Ding, Q.-L. Han, and X.-M. Zhang, "Distributed secondary control for active power sharing and frequency regulation in islanded microgrids using an event-triggered communication mechanism," *IEEE Trans. Ind. Inform.*, vol. 15, no. 7, pp. 3910–3922, Jul. 2019.

[8] A. K. Sahoo, K. Mahmud, M. Crittenden, J. Ravishankar, S. Padmanaban, and F. Blaabjerg, "Communication-less primary and secondary control in inverter-interfaced AC microgrid: An overview," *IEEE Trans. Emerg. Sel. Topics Power Electron.*, vol. 9, no. 5, pp. 5164–5182, Oct. 2021.

[9] Z. Zhang, C. Dou, D. Yue, and B. Zhang, "Predictive voltage hierarchical controller design for islanded microgrids under limited communication," *IEEE Trans. Circuits Syst. I, Reg. Papers*, vol. 69, no. 2, pp. 933–945, Feb. 2022.

[10] J. Chen, D. Yue, C. Dou, L. Chen, S. Weng, and Y. Li, "A virtual complex impedance based $(P - \dot{V})$ droop method for parallel-connected inverters in low-voltage AC microgrids," *IEEE Trans. Ind. Inform.*, vol. 17, no. 3, pp. 1763–1773, Mar. 2021.

[11] J. Zhou and P.-T. Cheng, "A modified $Q - \dot{V}$ droop control for accurate reactive power sharing in distributed generation microgrid," *IEEE Trans. Ind. Appl.*, vol. 55, no. 4, pp. 4100–4109, Jul./Aug. 2019.

[12] Y. Hu, J. Xiang, Y. Peng, P. Yang, and W. Wei, "Decentralised control for reactive power sharing using adaptive virtual impedance," *IET Gener. Transmiss. Distrib.*, vol. 12, no. 5, pp. 1198–1205, 2018.

[13] A. Rosini, A. Labella, A. Bonfiglio, R. Procopio, and J. M. Guerrero, "A review of reactive power sharing control techniques for islanded microgrids," *Renewable Sustain. Energy Rev.*, vol. 141, 2021, Art. no. 110745.

[14] B. Fan et al., "A novel droop control strategy of reactive power sharing based on adaptive virtual impedance in microgrids," *IEEE Trans. Ind. Electron.*, vol. 69, no. 11, pp. 11335–11347, Nov. 2022.

[15] H. Xu, X. Zhang, F. Liu, R. Shi, C. Yu, and R. Cao, "A reactive power sharing strategy of VSG based on virtual capacitor algorithm," *IEEE Trans. Ind. Electron.*, vol. 64, no. 9, pp. 7520–7531, Sep. 2017.

[16] A. Vijay, N. Parth, S. Doolla, and M. C. Chandorkar, "An adaptive virtual impedance control for improving power sharing among inverters in islanded AC microgrids," *IEEE Trans. Smart Grid*, vol. 12, no. 4, pp. 2991–3003, Jul. 2021.

[17] F. Deng, X. Li, X. Zhang, and P. Mattavelli, "An iterative virtual impedance regulation strategy in islanded microgrids for enhanced balanced, unbalanced and harmonic current sharing," *IEEE Trans. Sustain. Energy*, vol. 13, no. 1, pp. 514–526, Jan. 2022.

[18] I. Vechiu, O. Curea, and H. Camblong, "Transient operation of a four-leg inverter for autonomous applications with unbalanced load," *IEEE Trans. Power Electron.*, vol. 25, no. 2, pp. 399–407, Feb. 2010.

[19] A. Vijay, S. Doolla, and M. C. Chandorkar, "Varying negative sequence virtual impedance adaptively for enhanced unbalanced power sharing among DGs in islanded AC microgrids," *IEEE Trans. Energy Convers.*, vol. 36, no. 4, pp. 3271–3281, Dec. 2021.

[20] Y. Han, P. Shen, X. Zhao, and J. M. Guerrero, "An enhanced power sharing scheme for voltage unbalance and harmonics compensation in an islanded AC microgrid," *IEEE Trans. Energy Convers.*, vol. 31, no. 3, pp. 1037–1050, Sep. 2016.

[21] B. Sharma et al., "Power sharing in three-level NPC inverter based three-phase four-wire islanding microgrids with unbalanced loads," *IEEE Access*, vol. 11, pp. 20725–20740, 2023.

[22] E. Espina, R. Cardenas-Dobson, M. Espinoza-B, C. Burgos-Mellado, and D. Saez, "Cooperative regulation of imbalances in three-phase four-wire microgrids using single-phase droop control and secondary control algorithms," *IEEE Trans. Power Electron.*, vol. 35, no. 2, pp. 1978–1992, Feb. 2020.

[23] W. F. de Souza, M. A. Severo-Mendes, and L. A. Lopes, "Power sharing control strategies for a three-phase microgrid in different operating condition with droop control and damping factor investigation," *IET Renewable Power Gener.*, vol. 9, no. 7, pp. 831–839, 2015.

[24] *IEEE Standard for Interconnecting Distrib. Resour. With Electric Power Syst.*, IEEE Std 1547-2003, Jul. 28, 2003, pp. 1–28.

[25] M. Kosari and S. H. Hosseinian, "Decentralized reactive power sharing and frequency restoration in islanded microgrid," *IEEE Trans. Power Syst.*, vol. 32, no. 4, pp. 2901–2912, Jul. 2017.

[26] M. Eskandari, L. Li, M. H. Moradi, P. Siano, and F. Blaabjerg, "Active power sharing and frequency restoration in an autonomous networked microgrid," *IEEE Trans. Power Syst.*, vol. 34, no. 6, pp. 4706–4717, Nov. 2019.

[27] J. Zhang, J. Shu, J. Ning, L. Huang, and H. Wang, "Enhanced proportional power sharing strategy based on adaptive virtual impedance in low-voltage networked microgrid," *IET Gener., Transmiss. Distrib.*, vol. 12, no. 11, pp. 2566–2576, 2018.

[28] M. M. A. Abdelaziz, H. E. Farag, and E. F. El-Saadany, "Optimum droop parameter settings of islanded microgrids with renewable energy resources," *IEEE Trans. Sustain. Energy*, vol. 5, no. 2, pp. 434–445, Apr. 2014.

[29] M. Esmaeili, M. Sedighizadeh, and M. Esmaili, "Multi-objective optimal reconfiguration and DG (distributed generation) power allocation in distribution networks using big bang-big crunch algorithm considering load uncertainty," *Energy*, vol. 103, pp. 86–99, 2016.

[30] M. M. A. Abdelaziz, H. E. Farag, E. F. El-Saadany, and Y. A.-R.I. Mohamed, "A novel and generalized three-phase power flow algorithm for islanded microgrids using a newton trust region method," *IEEE Trans. Power Syst.*, vol. 28, no. 1, pp. 190–201, Feb. 2013.

[31] Y. Song, S. Sahoo, Y. Yang, and F. Blaabjerg, "Stability constraints on reliability-oriented control of ac microgrids–theoretical margin and solutions," *IEEE Trans. Power Electron.*, vol. 38, no. 8, pp. 9459–9468, Aug. 2023.

[32] D. De and V. Ramanarayanan, "Decentralized parallel operation of inverters sharing unbalanced and nonlinear loads," *IEEE Trans. Power Electron.*, vol. 25, no. 12, pp. 3015–3025, Dec. 2010.

[33] F. Ming, W. Gong, D. Li, L. Wang, and L. Gao, "A competitive and cooperative swarm optimizer for constrained multi-objective optimization problems," *IEEE Trans. Evol. Comput.*, vol. 27, no. 5, pp. 1313–1326, Oct. 2023.

[34] W. H. Kersting, "Radial distribution test feeders," *IEEE Trans. Power Del.*, vol. 6, no. 3, pp. 975–985, Aug. 1991.

[35] H. Han, Y. Liu, Y. Sun, M. Su, and J. M. Guerrero, "An improved droop control strategy for reactive power sharing in islanded microgrid," *IEEE Trans. Power Electron.*, vol. 30, no. 6, pp. 3133–3141, Jun. 2015.

Dalia Yousri received the B.Sc. (Hons.), M.Sc., and the Ph.D. degrees in electrical engineering from Fayoum University, Fayoum, Egypt, in 2011, 2016, and 2020, respectively.

She is an Assistant Professor with the Electrical Engineering Department, Fayoum University, Egypt. Since April 2022, she has been a Postdoctoral Fellow with the Advanced Power and Energy Research Center, Khalifa University, Abu Dhabi, UAE. Her current research interests include integrated energy management systems, modeling, analysis, and control of microgrids, as well as applications of optimization techniques in renewable energy-based systems. She is a Reviewer for various reputed journals, such as the IEEE TRANSACTIONS ON SUSTAINABLE ENERGY, IEEE TRANSACTIONS ON ENERGY CONVERSION, IEEE ACCESS, Elsevier Energy Conversion and Management, *International Journal of Hydrogen Energy, and Applied Energy.*

Dr. Yousri received an award of excellence in scientific research at Fayoum University for 2021. She is being recognized in the world's top 2% scientists list by Stanford University.

Hany E. Z. Farag (Senior Member, IEEE) received the B.Sc. (Hons.) and M.Sc. degrees in electrical engineering from Assiut University, Assiut, Egypt, in 2004 and 2007, respectively, and the Ph.D. degree in electrical and computer engineering from the University of Waterloo, Waterloo, ON, Canada, in 2013.

Since July 2013, he has been with the Department of Electrical Engineering and Computer Science, Lassonde School of Engineering, York University, where he is currently an Associate Professor and the York Research Chair in Integrated Smart Energy Grids. He is the Principal Investigator of the Smart Grid Research Laboratory funded from NSERC, Ontario Gov., MITACS, and several industry partners such as the IESO, Alectra Inc., EDA, TROES Inc., CUTRIC, and Hydrogenics. His current research interests include distributed and renewable energy resources, transportation electrification, green hydrogen generation and storage, microgrids, and applications of multiagent and blockchain technologies in smart grids.

Dr. Farag is a Registered Professional Engineer in Ontario and a recipient of the Early Researcher Award from the Government of Ontario.

Ahmed Al-Durra (Senior Member, IEEE) received the B.Sc., M.Sc., and Ph.D. degrees in electrical and computer engineering from Ohio State University, Columbus, OH, USA, in 2005, 2007, and 2010, respectively.

He is a Professor with the Electrical Engineering & Computer Science Department, Khalifa University, UAE. He is also the Associate Provost for Research at Khalifa University. His research interests include applications of control and estimation theory on power systems stability, micro and smart grids, renewable energy systems and integration, and process control. He has over 350 scientific articles in top-tier journals and refereed international conference proceedings. He has supervised/cosupervised over 35 Ph.D./Master's students. He is leading the Energy Systems Control & Optimization Lab under the Advanced Power & Energy Center, an Editor for IEEE TRANSACTIONS ON SUSTAINABLE ENERGY and IEEE POWER ENGINEERING LETTERS, and an Associate Editor for IEEE TRANSACTIONS ON INDUSTRY APPLICATIONS.

Hatem H. Zeineldin (Senior Member, IEEE) received the B.Sc. and M.Sc. degrees in electrical engineering from Cairo University, Giza, Egypt, in 1999 and 2002, respectively, and the Ph.D. degree in electrical and computer engineering from the University of Waterloo, Waterloo, ON, Canada, in 2006.

He was with Smith and Andersen Electrical Engineering Inc., North York, ON, USA, where he was involved in projects involving distribution system designs, protection, and distributed generation. He was a Visiting Professor with the Massachusetts Institute of Technology, Cambridge, MA, USA. He is currently with Khalifa University, Abu Dhabi, UAE, and also with the Faculty of Engineering, Cairo University. His current research interests include distribution system protection, distributed generation, and microgrids.

Ehab F. El-Saadany (Fellow, IEEE) received the B.Sc. and M.Sc. degrees in electrical engineering from Ain Shams University, Cairo, Egypt, in 1986 and 1990, respectively, and the Ph.D. degree in electrical engineering from the University of Waterloo, Waterloo, ON, Canada, in 1998,

He was a Professor with the ECE Department till 2019, where he was the Director of the Power MEng program between 2010 and 2015. He is currently a Professor with the Department of Electrical Engineering and Computer Science and the Director of the Advanced Power and Energy Research Center, Khalifa University, UAE. He is an internationally recognized expert in the area of sustainable energy integration and smart distribution systems. His research interests include smart grid operation and control, microgrids, transportation electrification, self-healing, cyber-physical security of smart grids, protection, power quality, and embedded generation.

Dr. El-Saadany is a Registered Professional Engineer in the Province of Ontario.